COMBINING NMR AND DENSITY LOGS FOR PETROPHYSICAL ANALYSIS IN GAS-BEARING FORMATIONS

R. Freedman, Chanh Cao Minh and Greg Gubelin
Schlumberger Oilfield Services

J.J. Freeman
Shell E&P Technology Company

Thal McGinness and Bob Terry
Amoco Production Company

David Rawlence
Woodside Offshore Petroleum

ABSTRACT

A new well logging method for evaluating gas-bearing reservoirs has been developed. The method combines total porosity from the CMR* Combinable Magnetic Resonance tool (TCMR) and density log-derived porosity (DPHI). It is based on new gas equations derived recently by Freedman (1997) and will be referred to as the Density–Magnetic Resonance (DMR) method. The equations and the method are also applicable to reservoirs with gas condensate or light oil near the wellbore. The method provides new petrophysical equations for (1) gas-corrected total formation porosity and (2) flushed-zone gas saturation. This paper describes the method in detail and applies it to the evaluation of field data.

The DMR gas-corrected total porosity (DMRP) is a new formation evaluation parameter. DMRP from the new method can be used in volumetric calculations to provide more accurate reservoir volume estimates than previously possible. Also, more accurate formation gas saturations can be computed when using gas-corrected total porosity in conjunction with deep-reading resistivity tools. The improved gas saturations and reservoir volumes provide better estimates of gas reserves. Gas-corrected total porosity can also be used in conjunction with the Coates-Timur equation to provide better permeability estimates in gas-bearing zones.

Attractive features of the DMR method include (1) faster logging in many environments because the gas polarization can be minimized, (2) robust gas evaluation because the separation in porosity is accentuated by the opposite effect of gas on the DPHI and NMR logs, (3) total porosity corrected for gas effect and (4) simple interpretation analogous to the familiar neutron-density gas detection.

The equations for gas-corrected total porosity and flushed-zone gas saturation are derived from the petrophysical response equations for total NMR porosity and formation bulk density. In gas-bearing reservoirs, gas-corrected total porosity is shown to obey a simple approximate equation that can be used to make a semi-quantitative estimate of DMRP by visual inspection of DPHI and TCMR logs. The effects that uncertainties in input parameters have on the outputs of the gas equations are studied using equations derived in Appendix A. Numerical examples using synthetic data and field data are used to demonstrate the relative insensitivity of the gas equation outputs to uncertainties in the inputs.

The method is applied to field logs from three commercial gas and oil wells. In the first field example the gas effect on the neutron log is suppressed by thermal neutron absorbers and the neutron-density logs fail to show gas in a gas-bearing zone. The large separation between DPHI and TCMR identifies the zone as gas bearing. In the second field example, gas-corrected total porosity logs are compared to neutron-density logs and to porosity measurements on conventional core. Logs of gas-corrected total porosity including the uncertainties

*Mark of Schlumberger

caused by uncertainties in the input parameters are displayed with core porosity to illustrate the robustness and accuracy of the method. A log of permeability derived using gas-corrected total porosity in the Coates-Timur equation is shown to provide excellent agreement with core permeabilities. The third field example uses the DMR method to evaluate a gas-bearing zone and a low-resistivity oil sand that lies below the gas sand.

INTRODUCTION

The recent introduction of total NMR porosity measurements into the well logging industry has provided many new formation evaluation techniques (Prammer *et al.*, 1996; Freedman *et al.*, 1997; Coates *et al.*, 1997). This paper introduces a new NMR interpretation method for the evaluation of gas-bearing formations. This new method is based on equations recently derived by Freedman (1997) and is referred to as the Density–Magnetic Resonance (DMR) method.

The DMR method combines petrophysical response equations for total CMR porosity (TCMR) and formation bulk density measurements to derive new equations for (1) gas-corrected total formation porosity and (2) flushed-zone gas saturation.

The physical basis underlying the DMR method can be understood by considering the TCMR and density log responses in a gas zone. If there is gas near the wellbore, density log-derived porosity (DPHI) overestimates total formation porosity because the measured formation bulk density is reduced by the presence of the gas. The presence of gas has the opposite effect on TCMR, which will underestimate the total formation porosity because of two effects: (1) the low hydrogen index of gas and (2) insufficient polarization of the gas. The reduced hydrogen index effect of gas is familiar to log analysts because it also causes neutron tool porosities to be reduced in gas zones. The insufficient polarization of gas occurs because reservoir gas has apparent longitudinal relaxation times ($T_{1,g}$) that are typically in the range from 3 to 6 sec at reservoir conditions. To fully polarize reservoir gas requires logging with Carr-Purcell-Meiboom-Gill (CPMG) sequences with wait times of the order of 10 sec. Such long wait times are impractical for routine logging operations because they result in very slow logging speeds.

Thus, in zones with gas near the wellbore, TCMR logs will read lower than DPHI logs. The difference or deficit between the two logs is proportional to the gas saturation and the effect is analogous to the neutron-density crossover effect in gas zones.

The new DMR method provides some advantages over the traditional neutron-density combination for evaluation of gas-bearing zones. First, the use of the neutron-density log response for gas detection is not always reliable because the effects of shale and thermal neutron absorbers on the neutron log response can suppress the crossover effect. Under these conditions, the DMR method provides a more robust gas signal because the NMR log responds only to the fluids in the formation and is less affected by mineralogy.

Second, in combining different measurements it is desirable that the tools investigate the same formation volume (i.e., in the radial, vertical and azimuthal directions). In this regard the vertical resolution and azimuthal coverage of the CMR tool closely matches that of the density tool (Casu, Andreani and Klopf 1998). Because of filtrate invasion it is also advantageous to combine measurements that have closely matched depths of investigation. Shallow-reading NMR devices such as the CMR tool are well matched to the depth of investigation of density tools. Figure 1 contains a plot of the integrated radial response functions for CMR, density and thermal neutron tools. If one uses the 50% response points for the depths of investigation (DOI), then the CMR, density and thermal neutron tools in Fig. 1 have respective DOIs of approximately 1, 2 and 6 in.

NMR-Only Gas Detection Methods– Most of the published methods for using NMR data for the detection and quantification of hydrocarbons are NMR-only methods. These methods include the Differential Spectrum Method (DSM) and the Shifted Spectrum Method introduced in a paper by Akkurt *et al.* (1995). A time domain implementation of the DSM known as the Time Domain Analysis method was developed by Prammer *et al.* (1995). The Echo Ratio Method was developed by Flaum, Kleinberg and Hürlimann (1996). Applications of NMR-only methods have been reported by Moore and Akkurt (1996) and by Akkurt, Moore and Freeman (1997).

Features of the DMR Method– The new method has some attractive features:

- Simplified gas detection is analogous to neutron-density crossover.
- Gas-corrected total porosity and flushed-zone gas saturation are computed from simple exact formulas.
- Outputs are insensitive to uncertainties in the input parameters.
- The gas phase polarization can be minimized so that shorter wait times and therefore faster logging speeds are possible.
- The method does not depend on the NMR tool gradients and therefore works equally well for gradient tools such as the MRIL† or saddle point tools such as the CMR. In reservoir rocks that have strong internal field gradients the data from NMR-only methods can be misinterpreted.

SOLUTION OF EQUATIONS FOR NMR AND BULK DENSITY MEASUREMENTS

The equations for gas-corrected total formation porosity and gas saturation are derived from the simultaneous solution of the petrophysical response equations for the formation bulk density and NMR measurements; i.e.,

$$\rho_b = \rho_{ma}(1-\phi) + \rho_f \phi (1 - S_{g,xo}) + \rho_g \phi\, S_{g,xo} \qquad (1)$$

for the bulk density and

$$\mathrm{TCMR} = \phi\, S_{g,xo} (HI)_g P_g + \phi (1 - S_{g,xo})(HI)_f \qquad (2)$$

for the total NMR porosity. The following quantities have been defined:

ρ_b = measured formation bulk density (g/cm^3).

ρ_{ma} = formation matrix density (g/cm^3).

ρ_f = density of liquid phase in the flushed zone at reservoir conditions (g/cm^3).

ρ_g = density of gas at reservoir conditions (g/cm^3).

ϕ = total formation porosity.

$(HI)_g$ = hydrogen index of gas at reservoir conditions.

$(HI)_f$ = hydrogen index of liquid phase in the flushed zone at reservoir conditions.

$S_{g,xo}$ = flushed-zone gas saturation.

$P_g \equiv 1 - \exp(-\frac{W}{T_{1,g}})$ = gas polarization function.

W = wait time for CPMG pulse sequence (s).

$T_{1,g}$ = gas longitudinal relaxation time at reservoir conditions (s).

The response Eqs. 1 and 2 describe a two-fluid model of a porous formation that consists of a rock matrix and a pore space filled with a liquid and a gas phase. The liquid phase is assumed to be a mixture of mud filtrate and formation water. Equation 1 for the measured formation bulk density is a volume-weighted average of the densities of the constituents of the formation. TCMR in Eq. 2 is equal to a volume-weighted average of the fractional contributions from each fluid component. The fractional contribution of each fluid to TCMR is the product of the hydrogen index of the fluid and its polarization function. In writing Eq. 2, it has been assumed that the wait time for the CPMG pulse sequence is sufficiently long to polarize the mud filtrate and formation water. Therefore, the polarization function of the liquid phase in Eq. 2 has been set equal to one.

The simultaneous solution of Eqs. 1 and 2 for the total formation porosity (ϕ) and the flushed-zone gas saturation ($S_{g,xo}$) is straightforward. To simplify the algebra a new parameter

$$\lambda = \frac{\rho_f - \rho_g}{\rho_{ma} - \rho_f} \qquad (3)$$

is defined and the bulk density is eliminated by introducing the density-derived porosity

$$\mathrm{DPHI} = \frac{\rho_b - \rho_{ma}}{\rho_f - \rho_{ma}}. \qquad (4)$$

The parameter λ is proportional to the density difference between the gas and liquid phases and is responsible for the gas effect on the density log porosity. One finds in Freedman (1997) that

$$\phi = \frac{\mathrm{DPHI} * (1 - \frac{(HI)_g * P_g}{(HI)_f}) + \frac{\lambda * \mathrm{TCMR}}{(HI)_f}}{(1 - \frac{(HI)_g * P_g}{(HI)_f}) + \lambda} \qquad (5)$$

†Mark of Numar Corporation

for the total formation porosity and

$$S_{g,xo} = \frac{\mathrm{DPHI} - \dfrac{\mathrm{TCMR}}{(HI)_f}}{\mathrm{DPHI} * \left(1 - \dfrac{(HI)_g * P_g}{(HI)_f}\right) + \dfrac{\lambda * \mathrm{TCMR}}{(HI)_f}} \qquad (6)$$

for the flushed-zone gas saturation. The volume of gas in the flushed zone ($\phi S_{g,xo}$) is obtained by multiplication of Eqs. 5 and 6 and is given by

$$V_{g,xo} \equiv \phi\, S_{g,xo} = \frac{\mathrm{DPHI} - \dfrac{\mathrm{TCMR}}{(HI)_f}}{\left(1 - \dfrac{(HI)_g * P_g}{(HI)_f}\right) + \lambda}. \qquad (7)$$

Equation 5 for gas-corrected total porosity is applicable when there is a gas (or light hydrocarbon) effect on the DPHI-TCMR logs; i.e., when DPHI porosity is greater than TCMR. In the opposite case, gas-corrected total porosity is defaulted to TCMR and the gas saturation set to zero.

60-40 Rule for Gas-Corrected Porosity– Equations 5-7 are the main results of this paper. Equation 5 tells us that the gas-corrected total porosity is a weighted sum of DPHI and TCMR/$(HI)_f$; i.e., Eq. 5 has the form

$$\phi = \mathrm{DPHI} * w + (1 - w) * \frac{\mathrm{TCMR}}{(HI)_f}, \qquad (8)$$

where the weight (w) is given by

$$w = \frac{1 - \dfrac{(HI)_g * P_g}{(HI)_f}}{\left(1 - \dfrac{(HI)_g * P_g}{(HI)_f}\right) + \lambda}. \qquad (9)$$

In practice the hydrogen indices of formation waters, water-base mud filtrates and oil-base mud filtrates are nearly equal to one so that $(HI)_f \cong 1$. Therefore, in a gas-bearing zone Eq. 8 tells us that the gas-corrected total porosity always lies between DPHI and TCMR. The weight in Eq. 9 depends on rock matrix and fluid densities (from Eq. 3) and on $(HI)_g$, $T_{1,g}$ and the CPMG pulse-sequence wait time (W). Our experience with these equations suggests an approximation that can be used for a quick estimate of gas-corrected porosity. Under typical conditions in a gas-bearing reservoir, a good approximation in Eq. 8 is to set $w \cong 0.6$, $(1-w) \cong 0.4$ and $(HI)_f \cong 1$. This can be verified by computing the weights in Eq. 9 using typical values for the parameters. Using this approximation leads to

$$\mathrm{DMRP} \cong 0.6 * \mathrm{DPHI} + 0.4 * \mathrm{TCMR}, \qquad (10)$$

where DMRP is the gas-corrected total porosity. Equation 10 provides a simple rule that can be used to estimate gas-corrected total porosity by visual inspection of TCMR and DPHI logs. The larger weight on DPHI results because there is a smaller gas effect on DPHI than on TCMR, as is shown in Appendix B by analysis of Eqs. 1 and 2 together with Eq. 4 for DPHI.

Applicability of Gas Equations– It is worth noting that the above equations are not restricted to shaly sand or simple carbonate reservoirs; i.e., formations consisting primarily of a single lithology such as sandstone, limestone or dolomite. Equations 5-7 are applicable to complex formations with mixed lithology provided that the matrix densities are known from core measurements or can be estimated from other log measurements.

It is also worth mentioning again that in deriving Eqs. 5-7 it was assumed that the wait time is sufficiently long to polarize the liquid phase. If this is not the case then one can apply an approximate correction by including a polarization function P_f in the last term of Eq. 2. With this modification Eqs. 5-7 retain the same form except that $(HI)_f$ is replaced everywhere by the product $(HI)_f * P_f$. If the well is drilled with oil-base mud and the reservoir is at irreducible water saturation, then TCMR can be corrected for insufficient wait time by applying an oil-base mud filtrate (OBMF) polarization correction to the free-fluid porosity. The corrected TCMR can be used in Eqs. 5-7. Although corrections for insufficient polarization of the mud filtrate can be applied, it is recommended that a job planner be used prior to logging to help select a wait time that ensures polarization of the filtrate.

Uncertainties in Input Parameters– The inputs to Eqs. 5-7 in each gas-bearing zone are (1) the NMR properties and bulk densities of the fluids in the formation, (2) the formation matrix density, (3) the measured formation bulk densities and (4) the total NMR porosities. The NMR properties of the fluids and the fluid densities depend on fluid type, reservoir temperature and pressure. For bulk fluids these properties can be estimated

from published charts and literature data (Akkurt *et al.*, 1995; Kleinberg and Vinegar, 1996). A recent paper by Straley (1997) has shown, contrary to conventional wisdom on gas wettability, that methane gas longitudinal relaxation times in rocks are reduced from their bulk values by surface relaxation. This adds additional uncertainty to our estimation of the *in-situ* NMR relaxation times of reservoir gas. The following paragraphs discuss how uncertainties in the input parameters propagate through Eqs. 5-7 and cause uncertainties in the outputs; e.g., ϕ , $S_{g,xo}$, $V_{g,xo}$. It is shown using synthetic data that these outputs are relatively insensitive to realistic input uncertainties of the magnitude that exist in practical applications.

Propagation of Uncertainties– The eight inputs to Eqs. 5-7 are ρ_b , ρ_{ma}, ρ_f, ρ_g, $T_{1,g}$, $(HI)_g$, $(HI)_f$, and TCMR. The uncertainties in the outputs of Eqs. 5-7 (i.e., ϕ, $S_{g,xo}$, $V_{g,xo}$) can be computed from the uncertainties assigned to each of the eight inputs. The uncertainties assigned to each input depend on the logging environment. For example, in a shaly sand development well a log analyst or geologist might reasonably assign a value to the formation matrix density that assumes a small uncertainty; e.g., ρ_{ma} = 2.65 ± 0.03 g/cm^3. In a shaly sand exploration well with unknown mineralogy the formation matrix density might reasonably be assigned a greater uncertainty; e.g., ρ_{ma} = 2.65 ± 0.05 g/cm^3. The uncertainties in the parameter inputs to petrophysical response equations usually reflect our lack of detailed knowledge of a particular parameter. There are also uncertainties in measured log responses. These are due to measurement errors and to statistical errors arising from random noise. For example, the formation bulk density tool measurement has a total measurement uncertainty of ±0.01 g/cm^3.

Examples of Error Analysis Using Synthetic Data– Tables 1A and 1B contain inputs and outputs, respectively, for 12 numerical examples computed using synthetic data. These examples are appropriate for a high-porosity shaly gas sand formation. These examples illustrate the magnitude of the errors in ϕ and $V_{g,xo}$ that are caused by realistic uncertainties in the input variables. In Tables 2A and 2B, analogous examples of inputs and outputs, respectively, for a low-porosity shaly gas sand are shown. The outputs in Tables 1B and 2B were computed using the synthetic input data in Tables 1A and 2A, respectively, and the equations in Appendix A.

Examples 1-3 in Table 1A are appropriate for a high-porosity shaly gas sand for which it has been assumed that the matrix density is known to within ±0.03 g/cm^3. Examples 4-6 are identical to Examples 1-3 except that the wait time of the pulse sequence has been reduced to 2 sec. In Examples 7-12 larger uncertainties have been assigned to the matrix density and also to TCMR. The outputs of the gas equations (Eqs. 5-7) and error analysis are shown in Table 1B. For the data in Table 1A, the uncertainties $\sigma(\phi)$ are in the range from 1.3 to 1.9 p.u. and the uncertainties $\sigma(V_{g,xo})$ vary from 2.0 to 2.9 p.u.

Tables 2A and 2B contain synthetic data inputs and outputs, respectively, that are appropriate for a low-porosity shaly gas sand. Observe in Table 2B that gas volume uncertainties $\sigma(V_{g,xo})$ are of the same order of magnitude as gas volumes $V_{g,xo}$. This implies that definitive gas quantification is more difficult in low-porosity zones.

FIELD DATA

In this section the DMR method is applied to field data. On all logs discussed in this paper the gas-corrected total porosity is denoted by DMRP. Flushed-zone gas saturations and volumes are denoted by SGXO and VGXO, respectively.

Field Example 1– This example is from a South Texas shaly sand formation (Fig. 2). The well was drilled with a water-base mud. The CMR tool was logged at 600 ft/hr using a 1.3-sec wait time. Logs of TCMR, DMRP, DPHI, NPHI are shown in track 2. The interval from X418 to X433 ft is gas bearing. Note that the gas effect on the neutron log is suppressed by mineralogy effects. The large deficit between DPHI and TCMR identifies the zone as gas bearing. The flushed zone gas volumes (VGXO) computed from Eq. 7 are displayed in track 1. The gas-corrected porosity (DMRP) provides an accurate formation total porosity that can be used to improve gas reserve estimates and permeability estimates from the Coates-Timur equation.

Field Example 2– This example is from a gas well drilled offshore Australia in a shaly sand reservoir. The well was drilled with Nova Plus, a synthetic oil-base drilling mud. The well penetrated a massive gas reservoir and conventional cores were cut over the zones of interest. The CMR tool was logged with a 6-sec wait time to achieve polarization of most of the OBMF.

TCMR, DMRP, DPHI and NPHI logs are displayed in track 3 of Fig. 3. The gas-bearing interval from X217 to X262 ft is easily identified from the deficit between DPHI and TCMR. A strong gas effect on the neutron log is evident from the large crossover of DPHI and NPHI. A log of the flushed-zone gas saturation (SGXO) is shown in track 2 of Fig. 3.

Comparisons of core data with log data are shown in Fig. 4. DMRP and core porosities are displayed in track 2. The agreement between DMRP and core porosity is good. Also shown in track 2 are neutron-density total porosity logs computed using two popular transforms. The neutron-density total porosity underestimates the core porosities by 3 p.u. over some parts of the interval.

Figure 5 shows the standard deviations in DMRP and SGXO resulting from uncertainties in the inputs to the gas equations. Track 2 shows logs of DMRP and DMRP plus and minus one standard deviation. Note that DMRP and the core porosities agree to within the estimated uncertainties for most of the core data. The inputs and the uncertainties in the inputs that were used for this well are shown in Table 3.

Figure 6 shows logs from a lower zone in the well of field Example 2. Logs of TCMR, DMRP, DPHI and NPHI and core porosities are shown in track 4. Note the good agreement between the core and DMRP, especially in the gas-bearing interval X370 to X383 ft. Log-derived permeabilities computed from the Coates-Timur equation using DMRP for total formation porosity and core permeabilities are in excellent agreement, as shown in track 3.

Field Example 3– This example is from a deepwater well drilled in the Gulf of Mexico (GOM). The well was drilled with Syntek, a synthetic oil-base mud. The well deviation is 43° over the zones of interest that included gas-bearing sands overlying an oil sand. The well was logged while drilling (LWD) with the LWD ADN* Azimuthal Density and Neutron tools and the CDR* Compensated Dual Resistivity tool. The wireline logs that were run after drilling included the -200 version of the CMR tool and the MDT* Modular Formation Tester tool. The CMR and MDT tools were run on drillpipe because of the high deviation angle of the well. The well was logged with a 5-sec wait time to polarize most of the OBM.

Track 5 of Fig. 7 shows the DPHI, TCMR and DMRP porosity logs over a gas-bearing interval that overlies an oil zone. There is large separation between DPHI and TCMR in the gas-bearing zone from X220 to X265 ft. Although the DPHI measurements were made during drilling and the TCMR after drilling, the strong gas effect on TCMR suggests that any gas flushed during or after drilling migrated back prior to logging with the CMR tool. Track 1 shows the MDT pressure data plotted versus true vertical depth (TVD). The corresponding measured depths (MD) are plotted beside the TVD depths. The MDT data can be fit with three straight lines corresponding to different fluid densities. In the gas-bearing zone the lower pressure gradient (larger slope of the trend line) is due to the low gas density. The gas-oil contact (GOC) predicted by the MDT data is at the intersection of the gas and oil trend lines at a TVD of X915 ft in track 1. The GOC is at a measured depth (MD) of X270 ft. Track 3 shows the flushed- zone gas saturation (SGXO) above the GOC and the flushed-zone oil saturation (SOXO) below the GOC.

The parameters used in Eq. 6 to compute the gas and oil saturations are shown in Tables 4 and 5, respectively. The separation between DPHI and TCMR in the oil zone is due to the reduced hydrogen index of the oil caused by a high gas-oil ratio. Track 4 shows the phase-shift resistivity (PSR) from the CDR tool. Note that the resistivities in the oil sand are only a few ohm-meter. Low- resistivity oil zones are common in the GOM and are difficult to identify using conventional methods. The oil-water contact (OWC) from the computed flushed-zone oil saturations at X360 ft MD is below the intersection of the MDT oil and water trend lines (at X965 ft TVD or X340 ft MD). Note that the character of the T_2 distributions shown in track 6 is useful in differentiating the gas-bearing zone from the oil zone. Note that in the water sand below the OWC in track 5 there is no deficit between DPHI and TCMR.

CONCLUSIONS

This paper has introduced a powerful new technique called the Density–Magnetic Resonance (DMR) method for evaluating gas-bearing reservoirs. The DMR method combines density-derived porosity logs and total NMR porosity logs to derive (1) gas-corrected total porosity and (2) flushed-zone gas saturation. Gas-corrected total

porosity is a new formation evaluation parameter that provides accurate formation porosity in gas-bearing zones. It also improves permeability estimates made using the Coates-Timur equation in gas-bearing zones.

Attractive features of the DMR method include

- simple identification of gas analogous to neutron-density crossover
- gas-corrected total porosity and flushed-zone gas saturations computed from simple exact equations
- low sensitivity to uncertainties in gas density, liquid density and gas NMR properties
- faster logging of gas reservoirs in some environments
- equations and method that are applicable to mixed lithologies
- equations and method that can be used to evaluate zones with gas condensate and light oils.

ACKNOWLEDGMENTS

We wish to thank Austin Boyd for his support during the early development of this new technique. It is a pleasure to thank Kaniza Khan for her assistance with the uncertainty analysis. Finally, we owe thanks to Kees Castelijns, Keith Bartenhagen and Catherine Hyde for help in gathering the data used for the field examples.

REFERENCES

Akkurt, R., Vinegar, H.J., Tutunjian, P.N. and Guillory, A.J., 1995, NMR logging of natural gas reservoirs, Paper N, Transactions of the Society of Professional Well Log Analysts 36th Annual Logging Symposium.

Akkurt, R., Moore, M.A. and Freeman, J.J., 1997, Impact of NMR in the development of a deepwater turbidite field, Paper SS, Transactions of the Society of Professional Well Log Analysts 38th Annual Logging Symposium.

Casu, P.A., Andreani, M., and Klopf, W., 1998, Using consonant-measurement sensors for more accurate log interpretations, Transactions of the Society of Professional Well Log Analysts 39th Annual Logging Sysmposium.

Coates, G.R., Menger, S., Prammer, M. and Miller, D., 1997, Applying total and effective NMR porosity to formation evaluation, SPE Paper 38736, presented at the Society of Petroleum Engineers Annual Technical Conference and Exhibition.

Flaum, C., Kleinberg, R.L. and Hürlimann, M.D., 1996, Identification of gas with the Combinable Magnetic Resonance tool (CMR*), Paper L, Transactions of the Society of Professional Well Log Analysts 37th Annual Logging Symposium.

Freedman, R. and Ausburn, B.E., 1985, The Waxman-Smits equation for shaly sands: I. simple methods of solution; II. error analysis: *The Log Analyst*, March-April, p. 11-23.

Freedman, R., Boyd, A., Gubelin, G., McKeon, D., Morriss, C.E. and Flaum, C., 1997, Measurement of total NMR porosity adds new value to NMR logging, Paper OO, Transactions of the Society of Professional Well Log Analysts 38th Annual Logging Symposium.

Freedman, R., 1997, Gas-corrected porosity from density-porosity and CMR measurements, *in* How to use borehole nuclear magnetic resonance: *Oilfield Review*, v. 9, no. 2, p. 54.

Kleinberg, R.L. and Vinegar, H.J., 1996, NMR properties of reservoir fluids: *The Log Analyst*, November-December, p. 20-32.

Moore, M.A. and Akkurt, R., 1996, Nuclear magnetic resonance applied to gas detection in a highly laminated Gulf of Mexico turbidite invaded with synthetic oil filtrate, SPE Paper 36521, presented at the Society of Petroleum Engineers Annual Technical Conference and Exhibition.

Prammer, M.G., Mardon, D., Coates, G.R. and Miller, M.N., 1995, Lithology-independent gas detection by gradient-NMR logging, SPE Paper 30562, Transactions of the Society of Petroleum Engineers Annual Technical Conference and Exhibition.

Prammer, M.G., Drack, E.D., Bouton, J.C., Gardner, J.S., Coates, G.R., Chandler, R.N. and Miller, M.N., 1996, Measurements of clay-bound water and total porosity by magnetic resonance logging, SPE Paper 36522, presented at the Society of Petroleum Engineers Annual Technical Conference and Exhibition.

Sherman, H. and Locke, S., 1975, Depth of investigation of neutron and density sondes for 35-percent porosity sand, Paper Q, Transactions of the Society of Professional Well Log Analysts 16th Annual Logging Symposium.

Straley, C., 1997, An experimental investigation of methane in rock materials, Paper AA, Transactions of the Society of Professional Well Log Analysts 38th Annual Logging Symposium.

ABOUT THE AUTHORS

Dr. Robert (Bob) Freedman is an Engineering Advisor in the Magnetic Resonance Department at the Schlumberger Sugar Land Product Center. A biographical sketch can be found in Paper OO in the 1997 SPWLA Annual Meeting Transactions.

Chanh Cao Minh graduated from Liege University, Belgium with an MS in electrical engineering and joined Schlumberger in 1978. He has had Operations assignments in France, Norway, UK, Indonesia, China, Saudi Arabia and Kuwait. He also spent 3 years working on formation evaluation research at the Schlumberger-Doll Research Center in Ridgefield, Connecticut. Presently, he works at the Sugar Land Product Center as the Interpretation Support-Development Specialist for Magnetic Resonance Products. He is a member of SPE, SPWLA, and SEG.

Greg Gubelin is the CMR product champion, coordinating the training, market introduction and future direction of the CMR service. A biographical sketch can be found in Paper OO in the 1997 SPWLA Annual Meeting Transactions.

Dr. J. Justin Freeman is a Staff Research Physicist for Shell E&P Technology Company in Houston, Texas. A biographical sketch can be found in Paper SS in the 1997 SPWLA Annual Meeting Transactions.

Thalbert E. McGinness received his BS in math education from East Central Oklahoma State University in 1964 and a Masters of Natural Science from Eastern New Mexico University in 1969. He joined Schlumberger in 1969 working the Mid-Continent and later the Texas Gulf of Mexico. He was hired by Amoco in 1979 working areas from New Mexico to Pennsylvania. He is currently primarily assigned asStaff Petrophysicist SG dedicated to the Deep Water - GOM. He is a member of SPWLA and SPE and has served as an elected chapter officer in SPWLA in Corpus Christi and Houston.

Robert (Bob) Terry is currently a Petrophysical Associate working in international operations and doing NMR research for Amoco. After receiving a BS in physics with a minor in geophysics at the Georgia Institute of Technology in 1975, he joined Schlumberger as a field engineer in West Texas. He spent 3 years working in various open and cased-hole field engineering assignments prior to moving into a series of management and log interpretation positions. In 1988 he joined Amoco to perform international log analysis. He is a graduate of the Amoco Petrophysics training program, where in subsequent years he has taught log analysis. He is an active member of the SPWLA, having authored and coauthored several papers. He is also the current Chairman of the Log Characterization Consortium.

APPENDIX A: UNCERTAINTY ANALYSIS

This Appendix discusses the equations that are used to compute the uncertainties in the outputs of Eqs. 5-7 that are caused by uncertainties in the inputs.

Let $f(x_1,...,x_n)$ denote a function of n random variables x_n that each have a distribution of possible values. Here the function represents any one of the outputs of Eqs. 5-7. Let $\sigma^2(f)$ denote the variance of $f(x_1,...,x_n)$. It can be expressed in terms of a summation over the variances $\sigma^2(x_i)$ in each of the input variables; e.g.,

$$\sigma^2(f) \cong \sum_{i=1}^{n} \left(\frac{\partial f}{\partial x_i} \right)^2_{x_i^*} \sigma^2(x_i) \,. \qquad \text{(A.1)}$$

The partial derivatives in Eq. A.1 are evaluated at x_i^*, where the asterisk superscript is used to denote the "best estimate" for each of the variables. The best estimates are the statistical expectation values of the variables; however, in practice these values are the user-assigned inputs to parameters such as $T_{1,g}$, $(HI)_g$ or measured values such as ρ_b and TCMR. In deriving Eq. A.1 it is assumed that errors in all the variables are statistically independent and that third and higher order terms in the deviations, $x_i - x_i^*$, can be neglected. In Eq. A.1 the variance $\sigma^2(x_i)$ in each input is the square of the uncertainty assigned to that input. The variance $\sigma^2(f)$ is likewise the square of the uncertainty in f that results from

uncertainties in the inputs. A more detailed derivation of Eq. A.1 can be found in a paper by Freedman and Ausburn (1985).

The partial derivatives that are needed in Eq. A.1 to compute the standard deviations in the gas-corrected total porosities (ϕ) and flushed-zone gas volumes ($V_{g,xo}$) are listed below. A formula is also given for computing the standard deviations in the flushed-zone gas saturations ($S_{g,xo}$) using these results. To save space it is useful to first define several quantities that appear repeatedly in the partial derivative expressions. Let

$$N_1 \equiv \text{DPHI} - \frac{\text{TCMR}}{(HI)_f},\quad N_2 \equiv 1 - \frac{(HI)_g P_g}{(HI)_f},$$

$$\alpha \equiv \frac{(HI)_g}{(HI)_f}, \text{ and } D \equiv 1 - \frac{(HI)_g P_g}{(HI)_f} + \lambda.$$

Using the above definitions, the partial derivatives needed in Eq. A.1 to compute $\sigma(\phi)$ are

$$\frac{\partial \phi}{\partial \rho_b} = \frac{N_2}{D(\rho_f - \rho_{ma})}, \tag{A.2}$$

$$\frac{\partial \phi}{\partial \rho_f} = \frac{N_1 N_2 (\rho_g - \rho_{ma})}{D^2 (\rho_f - \rho_{ma})^2} + \frac{N_2 (\rho_{ma} - \rho_b)}{D (\rho_f - \rho_{ma})^2}, \tag{A.3}$$

$$\frac{\partial \phi}{\partial \rho_g} = \frac{N_1 N_2}{D^2 (\rho_{ma} - \rho_f)}, \tag{A.4}$$

$$\frac{\partial \phi}{\partial \rho_{ma}} = \frac{N_1 N_2 (\rho_f - \rho_g)}{D^2 (\rho_f - \rho_{ma})^2} + \frac{N_2 (\rho_b - \rho_f)}{D (\rho_f - \rho_{ma})^2}, \tag{A.5}$$

$$\frac{\partial \phi}{\partial T_{1,g}} = \frac{W \alpha \lambda N_1 e^{\frac{-W}{T_{1,g}}}}{T_{1,g}^2 D^2}, \tag{A.6}$$

$$\frac{\partial \phi}{\partial (HI)_f} = \frac{-\lambda \,\text{TCMR}}{D (HI)_f^2} + \frac{\lambda P_g N_1 \alpha}{D^2 (HI)_f}, \tag{A.7}$$

$$\frac{\partial \phi}{\partial (HI)g} = \frac{-P_g \lambda N_1}{D^2 (HI)_f}, \tag{A.8}$$

$$\frac{\partial \phi}{\partial \text{TCMR}} = \frac{\lambda}{D (HI)_f}. \tag{A.9}$$

The partial derivatives needed in Eq. A.1 to compute $\sigma(V_{g,xo})$ are

$$\frac{\partial V_{g,xo}}{\partial \rho_b} = \frac{1}{D(\rho_f - \rho_{ma})}, \tag{A.10}$$

$$\frac{\partial V_{g,xo}}{\partial \rho_f} = \frac{N_1 (\rho_g - \rho_{ma})}{D^2 (\rho_f - \rho_{ma})^2} + \frac{(\rho_{ma} - \rho_b)}{D (\rho_f - \rho_{ma})^2}, \tag{A.11}$$

$$\frac{\partial V_{g,xo}}{\partial \rho_g} = \frac{N_1}{D^2 (\rho_{ma} - \rho_f)}, \tag{A.12}$$

$$\frac{\partial V_{g,xo}}{\partial \rho_{ma}} = \frac{N_1 (\rho_f - \rho_g)}{D^2 (\rho_f - \rho_{ma})^2} + \frac{(\rho_b - \rho_f)}{D (\rho_f - \rho_{ma})^2}, \tag{A.13}$$

$$\frac{\partial V_{g,xo}}{\partial T_{1,g}} = -\frac{W \alpha N_1 e^{\frac{-W}{T_{1,g}}}}{T_{1,g}^2 D^2}, \tag{A.14}$$

$$\frac{\partial V_{g,xo}}{\partial (HI)_f} = \frac{\text{TCMR}}{D (HI)_f^2} - \frac{\alpha P_g N_1}{D^2 (HI)_f}, \tag{A.15}$$

$$\frac{\partial V_{g,xo}}{\partial (HI)_g} = \frac{P_g N_1}{D^2 (HI)_f}, \tag{A.16}$$

$$\frac{\partial V_{g,xo}}{\partial \text{TCMR}} = \frac{-1}{D (HI)_f}. \tag{A.17}$$

The partial derivatives of $S_{g,xo}$ are not displayed here since its variance $\sigma^2(S_{g,xo})$ can be computed from the equation

$$\sigma^2 (S_{g,xo}) = \frac{V_{g,xo}^2 \sigma^2 (\phi)}{\phi^4} + \frac{\sigma^2 (V_{g,xo})}{\phi^2}. \tag{A.18}$$

APPENDIX B: GAS EFFECT ON DPHI AND TCMR

This Appendix compares the gas effect on DPHI and TCMR and shows that there is a larger gas effect on TCMR. The larger gas effect on TCMR provides a physical explanation of the "60-40 rule" for gas-corrected total porosity. From Eq. 1, the shift in measured formation bulk density in a gas-bearing formation is

$$\Delta\rho_b = -\phi S_{g,xo}(\rho_f - \rho_g). \quad \text{(B.1)}$$

Note that the effect of gas is to decrease the bulk density and therefore to increase the density-derived porosity DPHI. Similarly from Eq. 2, the shift in TCMR in a gas-bearing formation is

$$\Delta(\text{TCMR}) = -\phi S_{g,xo}((HI)_f - (HI)_g P_g). \quad \text{(B.2)}$$

The shift in the density-derived porosity is

$$\Delta(\text{DPHI}) = \frac{\Delta\rho_b}{\rho_f - \rho_{ma}} = \frac{\phi S_{g,xo}(\rho_f - \rho_g)}{\rho_{ma} - \rho_f}. \quad \text{(B.3)}$$

Equations B.2 and B.3 show that the gas effect decreases TCMR and increases DPHI. The effect on both is proportional to $\phi S_{g,xo}$ but the shift caused by gas effect is larger on TCMR. This can easily be verified by using typical values in the above equations. For example, consider a gas-bearing shaly sand reservoir and assume $(HI)_f = 1$, $(HI)_g = 0.4$, $T_{1,g} = 3$ sec, $W = 1.3$ sec, $\rho_{ma} = 2.65$, $\rho_f = 1$, and $\rho_g = 0.2$. Using these values to compute the value of the factor that multiplies $\phi S_{g,xo}$ in Eq. B.2 one finds –0.86 for the shift factor in TCMR. From Eq. B.3 one finds 0.48 for the shift factor in DPHI. Thus, the shift in TCMR is 1.8 times larger than the shift in DPHI.

Table 1A: Synthetic Data Inputs for High-Porosity Shaly Gas Sand

Example	ρ_b	ρ_{ma}	ρ_f	ρ_g	$T_{1,g}$	$(HI)_g$	$(HI)_f$	TCMR	W
1	2.2±0.01	2.65±0.03	1.0±0.1	0.2±0.1	4.0±1.0	0.4±0.1	1.0±0.1	0.10±0.01	4.0
2	2.2±0.01	2.65±0.03	1.0±0.1	0.2±0.1	4.0±1.0	0.4±0.1	1.0±0.1	0.15±0.01	4.0
3	2.2±0.01	2.65±0.03	1.0±0.1	0.2±0.1	4.0±1.0	0.4±0.1	1.0±0.1	0.20±0.01	4.0
4	2.2±0.01	2.65±0.03	1.0±0.1	0.2±0.1	4.0±1.0	0.4±0.1	1.0±0.1	0.10±0.01	2.0
5	2.2±0.01	2.65±0.03	1.0±0.1	0.2±0.1	4.0±1.0	0.4±0.1	1.0±0.1	0.15±0.01	2.0
6	2.2±0.01	2.65±0.03	1.0±0.1	0.2±0.1	4.0±1.0	0.4±0.1	1.0±0.1	0.20±0.01	2.0
7	2.2±0.01	2.65±0.05	1.0±0.1	0.2±0.1	4.0±1.0	0.4±0.1	1.0±0.1	0.10±0.015	4.0
8	2.2±0.01	2.65±0.05	1.0±0.1	0.2±0.1	4.0±1.0	0.4±0.1	1.0±0.1	0.15±0.015	4.0
9	2.2±0.01	2.65±0.05	1.0±0.1	0.2±0.1	4.0±1.0	0.4±0.1	1.0±0.1	0.20±0.015	4.0
10	2.2±0.01	2.65±0.05	1.0±0.1	0.2±0.1	4.0±1.0	0.4±0.1	1.0±0.1	0.10±0.015	2.0
11	2.2±0.01	2.65±0.05	1.0±0.1	0.2±0.1	4.0±1.0	0.4±0.1	1.0±0.1	0.15±0.015	2.0
12	2.2±0.01	2.65±0.05	1.0±0.1	0.2±0.1	4.0±1.0	0.4±0.1	1.0±0.1	0.20±0.015	2.0

Table 1B: Synthetic Data Outputs for High-Porosity Shaly Gas Sand							
Example	**DPHI**	**TCMR***	ϕ	$V_{g,xo}$	$S_{g,xo}$	$\sigma(\phi)$	$\sigma(V_{g,xo})$
1	0.27	0.10	0.205	0.14	0.69	0.013	0.020
2	0.27	0.15	0.224	0.10	0.44	0.013	0.021
3	0.27	0.20	0.244	0.06	0.24	0.014	0.023
4	0.27	0.10	0.210	0.13	0.62	0.013	0.017
5	0.27	0.15	0.228	0.09	0.41	0.013	0.019
6	0.27	0.20	0.246	0.06	0.22	0.015	0.022
7	0.27	0.10	0.205	0.14	0.68	0.019	0.027
8	0.27	0.15	0.224	0.10	0.44	0.018	0.027
9	0.27	0.20	0.244	0.06	0.24	0.019	0.029
10	0.27	0.10	0.210	0.13	0.62	0.018	0.024
11	0.27	0.15	0.228	0.09	0.41	0.018	0.025
12	0.27	0.20	0.246	0.06	0.22	0.019	0.027
*Note that TCMR is an input							

Table 2A: Synthetic Data Inputs for Low-Porosity Shaly Gas Sand									
Example	ρ_b	ρ_{ma}	ρ_f	ρ_g	$T_{1,g}$	$(HI)_g$	$(HI)_f$	**TCMR**	**W**
1	2.5±0.01	2.65±0.03	1.0±0.1	0.2±0.1	4.0±1.0	0.4±0.1	1.0±0.1	0.07±0.01	4.0
2	2.5±0.01	2.65±0.03	1.0±0.1	0.2±0.1	4.0±1.0	0.4±0.1	1.0±0.1	0.06±0.01	4.0
3	2.5±0.01	2.65±0.03	1.0±0.1	0.2±0.1	4.0±1.0	0.4±0.1	1.0±0.1	0.05±0.01	4.0
4	2.5±0.01	2.65±0.03	1.0±0.1	0.2±0.1	4.0±1.0	0.4±0.1	1.0±0.1	0.07±0.01	2.0
5	2.5±0.01	2.65±0.03	1.0±0.1	0.2±0.1	4.0±1.0	0.4±0.1	1.0±0.1	0.06±0.01	2.0
6	2.5±0.01	2.65±0.03	1.0±0.1	0.2±0.1	4.0±1.0	0.4±0.1	1.0±0.1	0.05±0.01	2.0
7	2.5±0.01	2.65±0.05	1.0±0.1	0.2±0.1	4.0±1.0	0.4±0.1	1.0±0.1	0.07±0.015	4.0
8	2.5±0.01	2.65±0.05	1.0±0.1	0.2±0.1	4.0±1.0	0.4±0.1	1.0±0.1	0.06±0.015	4.0
9	2.5±0.01	2.65±0.05	1.0±0.1	0.2±0.1	4.0±1.0	0.4±0.1	1.0±0.1	0.05±0.015	4.0
10	2.5±0.01	2.65±0.05	1.0±0.1	0.2±0.1	4.0±1.0	0.4±0.1	1.0±0.1	0.07±0.015	2.0
11	2.5±0.01	2.65±0.05	1.0±0.1	0.2±0.1	4.0±1.0	0.4±0.1	1.0±0.1	0.06±0.015	2.0
12	2.5±0.01	2.65±0.05	1.0±0.1	0.2±0.1	4.0±1.0	0.4±0.1	1.0±0.1	0.05±0.015	2.0

II

Table 2B: Synthetic Data Outputs for Low-Porosity Shaly Gas Sand							
Example	DPHI	TCMR*	ϕ	$V_{g,xo}$	$S_{g,xo}$	$\sigma(\phi)$	$\sigma(V_{g,xo})$
1	0.09	0.07	0.083	0.017	0.21	0.012	0.018
2	0.09	0.06	0.079	0.025	0.32	0.012	0.018
3	0.09	0.05	0.075	0.033	0.44	0.012	0.017
4	0.09	0.07	0.083	0.016	0.19	0.012	0.017
5	0.09	0.06	0.080	0.023	0.29	0.012	0.016
6	0.09	0.05	0.076	0.031	0.41	0.012	0.016
7	0.09	0.07	0.083	0.017	0.21	0.019	0.027
8	0.09	0.06	0.079	0.025	0.32	0.019	0.027
9	0.09	0.05	0.075	0.033	0.44	0.019	0.027
10	0.09	0.07	0.083	0.016	0.19	0.019	0.025
11	0.09	0.06	0.080	0.023	0.29	0.019	0.025
12	0.09	0.05	0.076	0.031	0.41	0.019	0.025
*Note that TCMR is an input.							

Table 3: Inputs Parameters and Uncertainties Used For Field Example 2								
$\sigma(\rho_b)$	ρ_{ma}	ρ_f	ρ_g	$T_{1,g}$	$(HI)_g$	$(HI)_f$	σ(TCMR)	W
0.01	2.65±0.03	0.95±0.15	0.21±0.05	5.0±1.0	0.47±0.1	1.0±0.1	0.015	6.0

Table 4: Inputs Parameters and Uncertainties Used For Field Example 3 in Gas Zone								
$\sigma(\rho_b)$	ρ_{ma}	ρ_f	ρ_g	$T_{1,g}$	$(HI)_g$	$(HI)_f$	σ(TCMR)	W
0.01	2.65±0.03	0.9±0.05	0.2±0.05	3.0±1.0	0.5±0.1	1.0±0.1	0.015	5.0

Table 5: Inputs Parameters and Uncertainties Used For Field Example 3 in Oil Zone								
$\sigma(\rho_b)$	ρ_{ma}	ρ_f	ρ_o	$T_{1,o}$	$(HI)_o$	$(HI)_f$	σ(TCMR)	W
0.01	2.65±0.03	0.9±0.05	0.75±0.1	2.0±1.0	0.8±0.1	1.0±0.1	0.015	5.0

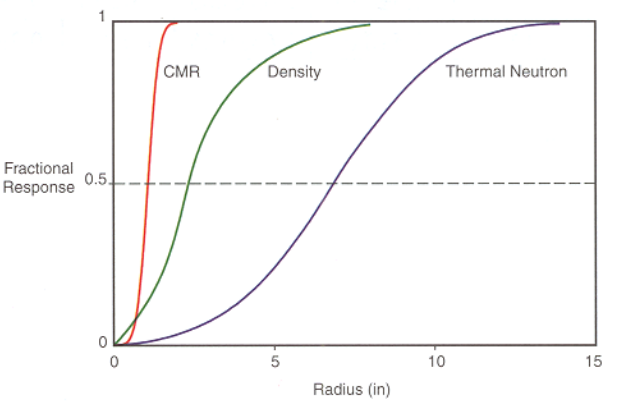

Figure 1. The integrated radial response functions for CMR, density, and thermal neutron tools. The dashed line intersects each curve at the radial depth from which 50% of the cumulative signal is derived. The response functions show that the CMR and density tools have better matched depths of investigation than do the density and thermal neutron tools. The density and thermal neutron response functions were measured in a 35-p.u. sandstone by Sherman and Locke (1975).

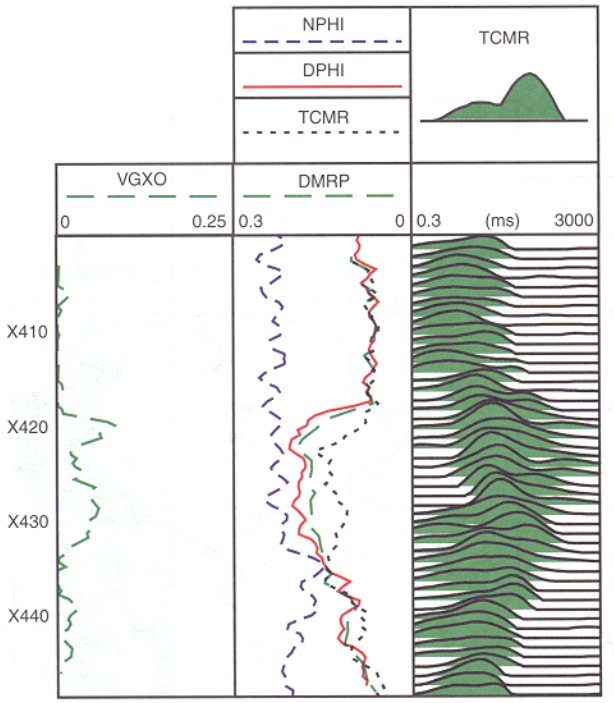

Figure 2. Logs from Example 1. The well is drilled in a South Texas shaly sand formation. TCMR, DMRP, DPHI and NPHI are displayed in track 2. The interval from X418 to X433 ft is gas bearing. Note that the neutron in this interval is reading high because of effects of thermal neutron absorbers. The large deficit between DPHI and TCMR clearly identifies the zone as gas bearing. The flushed-zone gas volumes (VGXO) computed from Eq. 7 are displayed in track 1. The gas-corrected porosity log (DMRP) computed from Eq. 5 provides an accurate formation porosity log that can be used to improve log-based estimates of gas reserves and formation permeability.

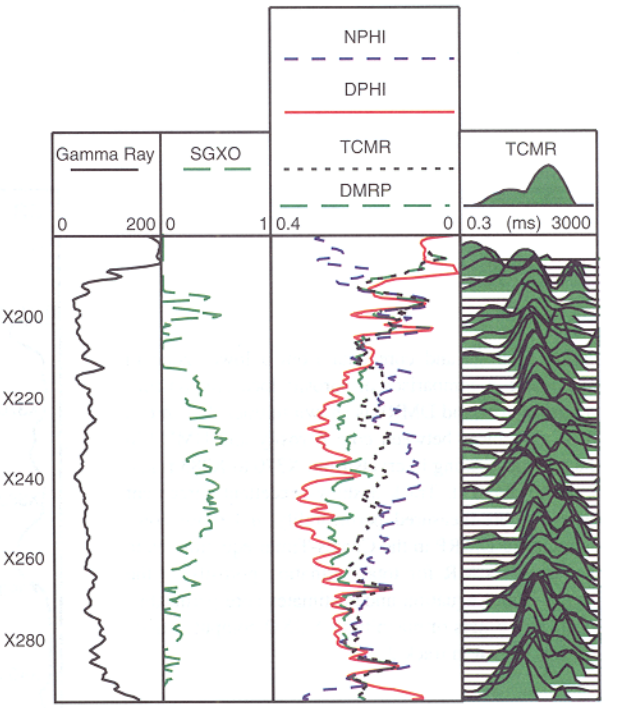

Figure 3. Logs from Example 2. These logs are from a well drilled Offshore Australia in a shaly sand formation. NPHI, DPHI, TCMR and DMRP logs are displayed in track 3. Note that the large deficit between the DPHI and TCMR in the interval X217 - X262 ft clearly identifies it as gas bearing. The NPHI and DPHI logs also exhibit a large gas effect in this interval. The gas-corrected total porosity (DMRP) computed from Eq. 5 is a new formation evaluation parameter. Track 2 displays the flushed-zone gas saturation computed from Eq. 6.

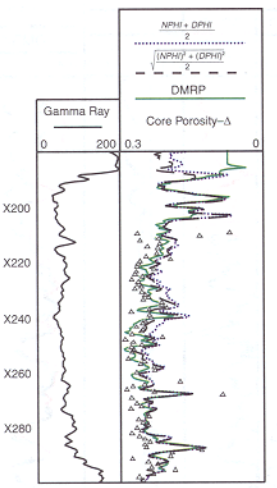

Figure 4. Logs and conventional core data from Example 2. A comparison of DMRP with core porosity is displayed in track 2. Also shown in track 2 are two popular transforms for combining DPHI and NPHI data to compute neutron-density crossplot porosity. Note the good overall agreement between DMRP and core porosity. The two DPHI-NPHI porosity logs underestimate core porosity by 3 p.u. in some sections.

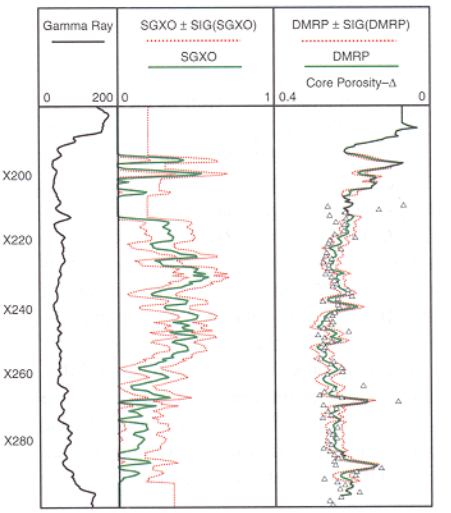

Figure 5. Logs and core porosities from Example 2. Track 3 shows a comparison of DMRP and core porosity. Also shown are the uncertainties (standard deviations) in DMRP caused by uncertainties in the input parameters used in Eq. 5. Flushed-zone gas saturations (SGXO) and uncertainties SIG(SGXO) caused by uncertainties in the input parameters used in Eq. 6 are shown in track 2. The input parameters and the uncertainties in the input parameters that were used for the analysis in Example 2 are shown in Table 3.

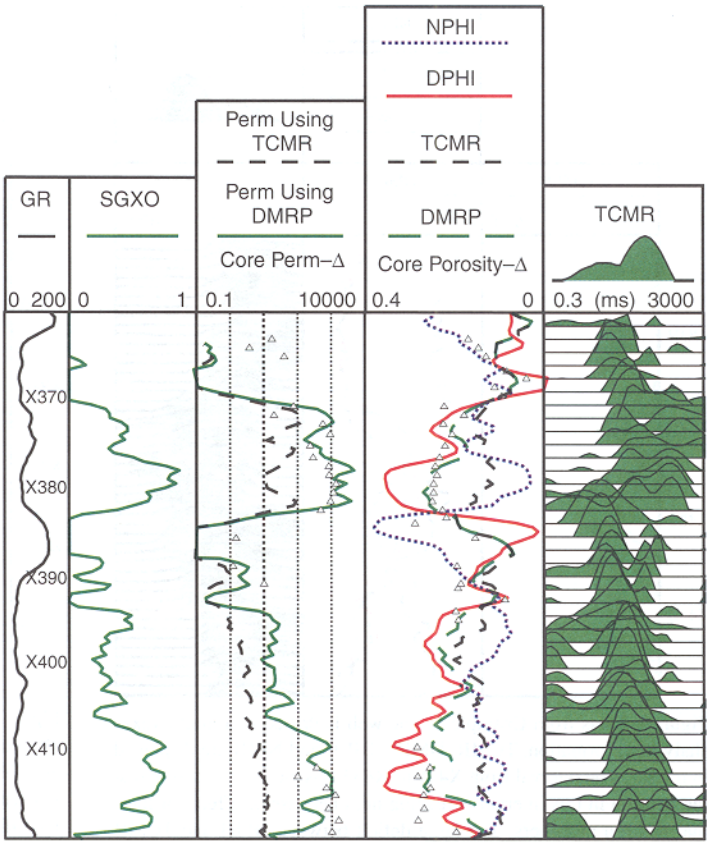

Figure 6. Logs and core data from a lower zone in Example 2. A comparison of porosity measured on conventional core and DMRP is shown in track 4. There is good agreement between core porosity and DMRP in the two gas-bearing intervals from X370 to X383 ft and X388 to X420 ft. Track 3 shows excellent agreement between core-measured permeability and those computed using DMRP in the Coates-Timur equation. Note that using TCMR for total formation porosity in the Coates-Timur equation underestimates core permeability by two orders of magnitude. SGXO computed from Eq. 6 is shown in track 2.

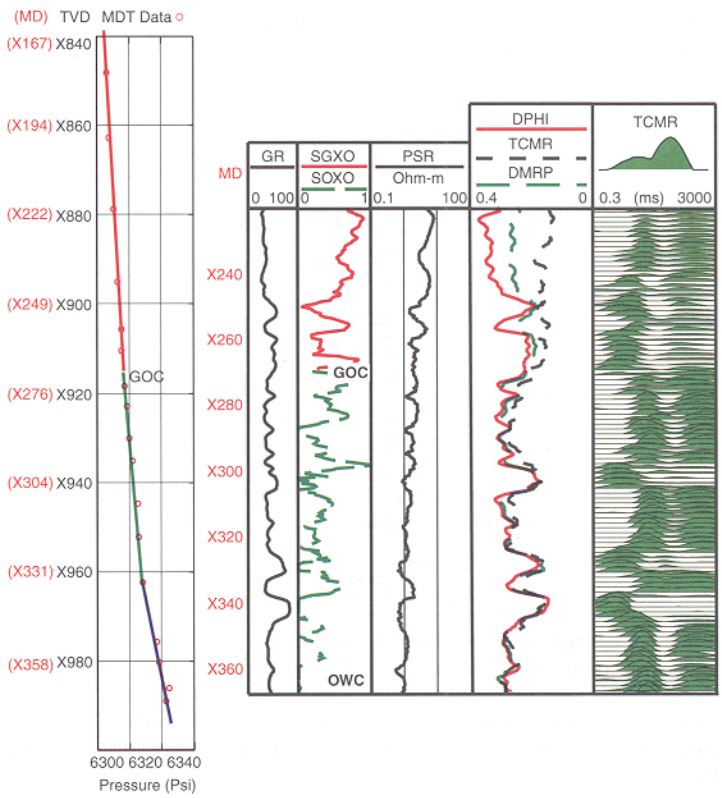

Figure 7. Logs from a deepwater Gulf of Mexico well. DPHI, TCMR and DMRP logs are shown in track 5. The separation between DPHI and TCMR in the upper section is indicative of a large gas effect on the density and NMR logs. Below the gas sand is a low-resistivity oil sand. The CDR phase-shift resistivity (PSR) log is shown in track 4. The DPHI-TCMR separation is smaller in the oil zone but still indicates the presence of the oil. The MDT pressure data and pressure gradient trend lines are shown in track 1. The pressure data shows the GOC to be at X270 ft measured depth (MD), which is consistent with the change at X270 ft in the character of the T_2 distributions. The flushed-zone hydrocarbon saturations in track 3 were computed using Eq. 6 and the input data in Tables 4 and 5.